Chapter 6. System Noise Analysis and Performance Optimization

As an optoelectronic measurement system, the performance of the SCIIB sensor is limited by the noises associated with each individual electronic and optical component and their combined effects. A detailed analysis of these noise effects on the system performance is a very important design step since it provides a guideline to achieve an optimal system performance. This chapter provides a detailed analysis of the noise performance of the single-mode fiber (SMF) SCIIB sensor system, including both the electronic noise and the optical noise. Based on the analysis results, performance improvement measures are proposed.

6.1 Electronic Noise of the SMF SCIIB System

Usually, the ultimate limit of the performance of an optoelectronic sensor system is associated with the receiving electronics used to interrogate the sensor. This can be further decomposed into two parts: 1) the fundamental photon noise limit (shot noise) of the photodetector, and 2) thermal noise of the electronics. In addition to the noise associated with the receiving electronics, the noise of the optical source, such as the optical power fluctuation and the source wavelength drift, can also cause measurement errors to the sensor system. Here the optical power fluctuation of the source is no longer a concern because as previously discussed in Chapter 2 the SCIIB sensor system can self-compensate for the source power fluctuation. The error caused by the optical wavelength drift of the source will be discussed in the next section as it is categorized to be part of the optical noise. Therefore this section will be devoted to the discussion of the electronic noise only.

6.1.1 Photodetector Noises

1. Shot noise

Shot noise of a photodetector is a manifestation of the fact that the electric current consists of a stream of electrons that are generated at random times. It was first studied by Schottky in 1918 and has been thoroughly investigated since then [92]. The photodiode current generated in response to a constant optical signal can be written as

$$\mathrm{I(t)} = I_p + i_s(t)\,, \tag{6-1}$$

where $I_p=RP_{in}$ is the average current and $i_s(t)$ is a current fluctuation related to shot noise. P_{in} is the input optical power to the photodetector and R is the responsivity of the photodetector.

Mathematically, $i_s(t)$ is a stationary random process with Poisson statistics which in practice can be approximated by the Gaussian statistics. The autocorrelation function of $i_s(t)$ is related to the spectral density $S_s(f)$ by the Wiener-Khinchin theorem

$$\langle i_s(t) i_s(t+\tau)\rangle = \int_{-\infty}^{\infty} S_s(f)\exp(2\pi i f\tau)df\ . \tag{6-2}$$

The spectral density of shot noise is constant and is given by $S_s(f)=qI_p$ (shot noise is called white for this reason). q is the charge on an electron (1.6×10^{-19} C). Note that $S_s(f)$ is a two-sided spectral density, as negative frequencies are also included in Equation (6-2). If only positive frequencies are considered by changing the lower limit of integration to zero, the one-sided spectral density becomes $2qI_p$.

The noise variance is obtained by setting τ=0 in Equation (6-2) and is given by

$$\sigma_s^{\,2} = \langle i_s^{\,2}(t)\rangle = 2qI_p\Delta f\ , \tag{6-3}$$

where Δf is the effective noise bandwidth of the receiver. The actual value of Δf depends on where the noise is measured and it is usually corresponds to the bandwidth of the amplifying circuits.

2. Dark current

All photodetectors generate some current noise even in the absence of an optical signal because of stray light or thermal generation of electron-hole pairs. This residual current is referred to as the dark current. Since the dark current I_d also generates shot noise, its contribution is included in the following equation

$$\sigma_s^{\,2} = 2q(I_p + I_d)\Delta f \tag{6-4}$$

3. Thermal noise

At a finite temperature, electrons in any conductor move randomly. Random thermal motion of electrons in a resistor manifests as a fluctuating current even in the absence of an applied voltage. The load resistor in the front end of an optical receiver adds such fluctuations to the current generated by the photodiode. This additional noise component is referred to as thermal noise. It is also called Johnson noise or Nyquist noise after the two scientists who first studied it experimentally and theoretically. Thermal noise can be defined as the current fluctuation $i_T(t)$. Mathematically, $i_T(t)$ is modeled as a stationary Gaussian random process with a spectral density that is frequency independent up to 1Thz (nearly white noise) and is given by [93]

$$S_T(f) = \frac{2k_B T}{R_L}, \tag{6-5}$$

where k_B is the Boltzmann constant (1.38×10^{-23}J/°K), T is the absolute temperature, and R_L is the load resistor. As mentioned before, $S_T(f)$ is also the two-sided spectral density.

The autocorrelation function of $i_T(t)$ is given by

$$\langle i_T(t) i_T(t+\tau)\rangle = \int_{-\infty}^{\infty} S_T(f)\exp(2\pi i f\tau)df \tag{6-6}$$

Therefore, the noise variance is obtained by setting $\tau=0$ and becomes

$$\sigma_s^{\,2} = \langle i_s^{\,2}(t)\rangle = \int_{-\infty}^{\infty} S_T(f)df = \frac{4k_B T}{R_L}\Delta f \tag{6-7}$$

where Δf is the effective noise bandwidth which is defined same as for the shot noise case.

6.1.2 Noise assumption at the transimpedance amplifier

The developed SCIIB system uses two transimpedance amplifiers to convert the optical current signals to the voltage outputs of the two channels. It is thus necessary to describe the noise performance of the transimpedance amplifier as it combines the shot noise and the thermal noise, and also introduce other noise to the final sensor output.

The noise equivalent circuit of the transimpedance amplifier (as shown in Figure 3-8) is given in Figure 6-1. The bandwidth of the transimpedance amplifier is *RC* limited and given by:

$$\Delta f = \frac{1}{2\pi R_f C_f}. \tag{6-8}$$

where R_f is the feedback resistance, and C_f is the feedback capacitance.

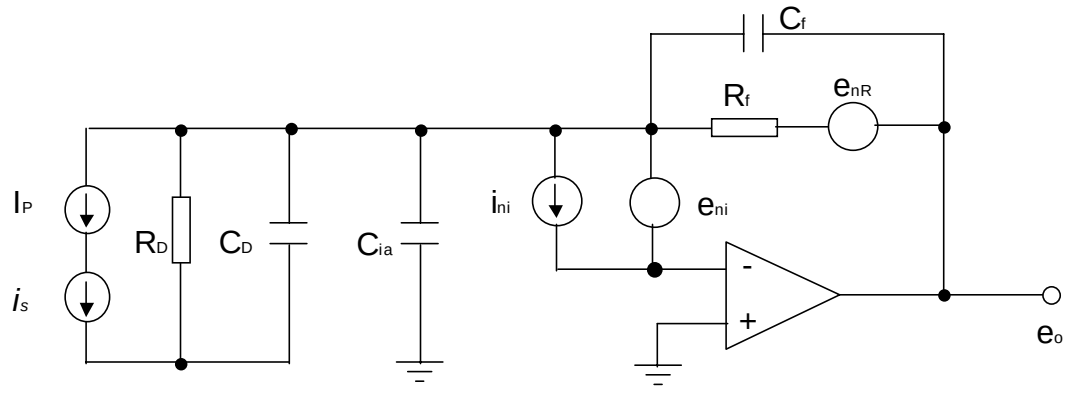

Figure 6-1. Noise equivalent circuit of the transimpedance amplifier

The output voltage (e_o) from the transimpedance amplifier can be calculated by

$$e_o = e_s + e_{no} = I_p R_f + e_{no}, \tag{6-9}$$

where e_s is the signal voltage of the amplifier, I_p is the signal generated photocurrent from the photodetector, and e_{no} is the voltage noise of the amplifier which includes the noise voltage generated by the shot noise of the detector, the thermal noise of the feedback resistor (e_{noR}), the amplifier's input current noise (e_{noi}), and the amplifier's input voltage noise (e_{noe}).

1. Effect of the photodetector shot noise

The shot noise generated at the photodetector (i_s) will be amplified by the feedback resistor and gives the corresponding voltage noise (e_{nos}) given by

$$e_{nos} = i_s R_f = \sqrt{2q(I_p + I_d)\Delta f}\, R_f \,. \tag{6-10}$$

2. Thermal noise of the feedback resistor

The thermal noise of the feedback resistor generates a voltage noise e_{noR} that can be expressed by

$$\mathrm{e}_{\mathrm{noR}} = \sqrt{4k_B T R_f \Delta f}\,. \tag{6-11}$$

3. Amplifier's input current noise

e_{noi} is the output noise components produced by the amplifier's input current noise ($i_{ni} = \sqrt{2qI_{B-}\Delta f}$) which is a shot noise produced by the input bias current I_{B-}. This noise current flows directly through the feedback resistor, producing a noise voltage of

$$\mathrm{e}_{\mathrm{noi}} = R_f \sqrt{2qI_{B-}\Delta f}\,. \tag{6-12}$$

Choosing a FET-input operational amplifier with an I_{B-} in the picoampere range generally makes this noise component negligible for practical levels of feedback resistance. For the AD795 operational amplifier, the input current noise is $I_{B-} = 13fA$.

4. Amplifier's input voltage noise

e_{noe} represents output noise components produced by the amplifier's input voltage noise. Within the response boundary of the op amp, this noise can be calculated by:

$$e_{noe} = \frac{1 + R_f C_i s}{1 + R_f C_f s} e_{ni} \quad . \tag{6-13}$$

This will be a high frequency noise when the capacitors dominate the noise gain. For the AD795 amplifier, $e_{ni}=3\mu v$ below 10Hz.

5. Total voltage noise

The total voltage noise (e_{no}) can be obtained by adding the contributions of all the above noises. Since these noises are independent random processes which can be approximately modeled by Gaussian statistics, the total variance of voltage fluctuation at the output of the transimpedance amplifier can be obtained by adding individual variances. Therefore, the combined output voltage noise of all components is given by

$$e_{no} = \sqrt{e^2_{nos} + e^2_{noR} + e^2_{noi} + e^2_{noe}} \quad . \tag{6-14}$$

6.1.3 Power budget of the developed SCIIB system

Assume that the maximum output power from the SLED source is 1.6 mW. The coupler introduces a loss of 6dB (75%) because of the double passes. The Fresnel reflection of the fiber endface is 4%. If counting for the two reflections at the sensor head, the total average reflected power will be 8% of the incident power. There are other losses associated with the SCIIB system. For example, the coupling loss of the fiber to the GRIN lens is about 0.2dB (4.5%). The beamsplitter splits the light into the two channels with a ratio of 50:50, which introduces another 50% power loss to each channel. The power seen by the narrow band channel will only be 25% of the original power of the full spectrum because the bandpass filter only slices a portion (10nm spectral width) of the

original source bandwidth (40nm). The bandpass filter used in the system also introduces an optical loss of 60%. The maximum operating distance for the single mode fiber sensor is 10km, which will introduce a fiber loss of 2×0.3dB/km×10km=6dB (74.88%) because of the double pass of the light, where 0.3dB/km is the assumed loss at λ=1310nm of the single-mode fiber used in connecting the sensor to the signal processing unit. Finally, it is wise to allow a loss margin of 10dB (90%) power loss for the fiber deployment. The loss items with their estimated values are listed in Table 6-1.

Table 6-1. Optical loss mechanisms in single-mode SCIIB system

Optical loss mechanisms	Value
Coupler loss ($\boldsymbol{L_C}$)	6dB (or 75%)
Average Fresnel reflection of the fiber ends ($\boldsymbol{r_f}$)	8%
GRIN lens pigtail loss ($\boldsymbol{L_{GRIN}}$)	0.2dB (or 4.5%)
Beamsplitter loss ($\boldsymbol{L_{BS}}$)	3dB (or 50%)
Filtering loss ($\boldsymbol{L_{ft}}$)	6dB (or 75%)
Bandpass filter efficiency ($\boldsymbol{\eta_{BP}}$)	60%
Fiber attenuation loss ($\boldsymbol{L_f}$)	10km × 0.3dB/km × 2 = 6dB (or 75%)
Loss margin for fiber deployment ($\boldsymbol{L_{Mrg}}$)	10dB (90%)

Therefore the optical power seen by the photodetector at the signal channel can be estimated to be

$$P_{in} = P_s \times (1 - L_c) \times r_f \times (1 - L_{GRIN}) \times (1 - L_{BS}) \times (1 - L_{ft}) \times \eta_{BP} \times (1 - L_f) \times (1 - L_{Mrg}) = 57.6nW \quad (6\text{-}15)$$

6.1.4 Signal-to-noise ratio estimation of SCIIB electronics

Based on the above analysis and the estimated optical power seen by the photodetectors of the SCIIB signal channel, we can calculate the estimated signal-to-noise ratio (SNR) of the developed SCIIB system, where SNR is defined as

$$SNR = 10\log(\frac{\text{average signal power}}{\text{noise power}}) = 20\log(\frac{\text{average signal voltage}}{\text{noise voltage}}) = 20\log(\frac{e_s}{e_{no}}) = 20\log(\frac{I_p R_f}{\sqrt{e^2_{nos} + e^2_{noR} + e^2_{noi} + e^2_{noe}}}) \quad , \qquad (6\text{-}16)$$

where we used the fact that electrical power varies as square of the voltage.

Table 6-2. SNR calculation of the single-mode fiber SCIIB electronics

Items	Value
Shot noise generated voltage noise ($\boldsymbol{e_{nos}}$)	5.28 (μV)
Thermal noise of the feedback resistor ($\boldsymbol{e_{noR}}$)	1.62 (μV)
Amplifier's input current noise ($\boldsymbol{e_{noi}}$)	2.57 (nV)
Amplifier's input voltage noise ($\boldsymbol{e_{noe}}$)	3 (μV)
Total noise voltage ($\boldsymbol{e_{no}}$)	6.28 (μV)
Average signal current ($\boldsymbol{I_p}$)	57.6nW × 0.95A/W = 54.7 (nA)
Dark current of the photodetector ($\boldsymbol{I_D}$)	15 (pA)
Average signal voltage ($\boldsymbol{e_s}$)	547 nA × $10^7\Omega$ = 0.547 (V)
Signal-to-noise ratio ($\boldsymbol{SNR}$)	98.8 (dB)
Equivalent normalized noise level	1.148×10^{-5}

Therefore, the signal-to-noise ratio of the electronics of the single-mode fiber SCIIB sensor system can be calculated as shown in Table 6-2, where the noise terms are listed separately. From the table, we can see that the theoretical signal-to-noise ratio of the receiving electronics of the single-mode fiber SCIIB system is about 98.8dB (equivalent

to a normalized noise level of 1.148×10^{-5}). This is, however, by no means the actual SNR of the entire system. As we will see in the analyses of next section, the optical noise will dominate the performance characteristics of the system.

6.2 Optical Noise Performance of SMF SCIIB System

As discussed in Chapter 3, the basic optical components in the SMF SCIIB sensor system include the optical source (SLED), fiber coupler, optical fibers, GRIN lens, beamsplitter, and optical bandpass filter. In order to achieve the desirable performance of the sensor system, it is necessary for those optical components to perform their functions accurately. Unfortunately, environmental perturbations, such as temperature changes and mechanical vibrations, can easily introduce noises to the system through the interaction between the optical components and the outside medium. These noises may cause the optical components to deviate from their desired functions and result in measurement errors. Therefore, it is the purpose of this section to examine the noise performance of the optical system to ensure a reliable optical design.

The interaction between the optical components and the environment disturbance could affect the optical performance of the component in four different aspects: intensity, phase, wavelength, and state of polarization (SOP). The resultant noise from these four aspects is system and component dependent. The SCIIB system is immune to the intensity noise since it has the full capability of self-compensation for the intensity fluctuation by taking the ratio of the two channels' outputs. The phase fluctuation of the optical components will not affect the system performance because the phase of the interference signal from the Fabry-Perot cavity purely depends on the sensor probe itself. The phase shift of the optical components only adds the same amount phase change to both of the interference components. This common phase shift will be eliminated from

the final interference signal of interest. The analysis can thus be narrowed down to the effects of wavelength drifts and changes of the state of polarization.

6.2.1 Wavelength Drift Induced Noise

The SCIIB system measures the pressure signal by monitoring the sensor cavity length change resultant from the applied pressure. Although the sensor cavity length change is read directly from the intensity change, the generation of the signal is based on the basic principle of optical interference. The interference of two optical waves is a sinusoidal function of the phase difference between these two waves, which is inversely proportional to the optical wavelength of the source. It can be imagined that wavelength drifts will introduce a change to the interference signal and result in measurement errors. Usually, the wavelength drift induced error can be analyzed directly from the interference equation. However, the case for the SCIIB system is somewhat different because it is the spectral characteristic of the optical filter that determines the interference signal. Therefore, a detailed investigation of the wavelength drift induced error needs more careful considerations.

1. Spectrum characteristic change of the optical bandpass filter

Without any doubt, the change of the spectrum after the optical bandpass filter will directly shift the interference signal. A careful examination of the system reveals that the wavelength drift before the optical bandpass filter can also cause an error through the non-centered filtering and the residual interference fringe in the reference channels.

The optical bandpass filter used in the SCIIB signal channel is a Fabry-Perot type multilayer thin film filter. The spectrum characteristics of the filter are dependent on the thickness and the refractive index of the multilayer thin film, which will change with the ambient temperature because of the thermal expansion effect and the temperature dependence of the refractive index. Assuming that the center wavelength of the filter has

a temperature sensitivity of 0.001nm/°C, a temperature change of 70°C (from -15°C to 55°C) will cause a maximum change of 0.07nm in the center wavelength.

Taking the derivative of both sides of Equation (2-11) with respect to λ, we have

$$\frac{ds}{d\lambda} = -\gamma \frac{4\pi L}{\lambda^2} \sin(\frac{4\pi}{\lambda} L) . \tag{6-17}$$

The wavelength drift induced error can thus be calculated by

$$\delta s = abs\left\{ \gamma \frac{4\pi L}{\lambda^2} \sin(\frac{4\pi}{\lambda} L)\delta\lambda \right\}, \tag{6-18}$$

which reaches the maximum at the quadrature points where the sinusoidal function gives its maximum values of ±1. Therefore,

$$\delta s_{\max} = \gamma \frac{4\pi L}{\lambda^2} \delta\lambda . \tag{6-19}$$

In Chapter 2, we also defined the operating range of the SCIIB system given in Equation (2-14). Therefore, the normalized error can be calculated by

$$\frac{\delta s_{\max}}{\Delta s_{\max}} = \frac{\gamma \frac{4\pi L}{\lambda^2} \delta\lambda}{1.6\gamma} = \frac{4\pi L}{1.6\lambda^2} \delta\lambda \ . \tag{6-20}$$

The normalized error resultant from the wavelength drift of the optical filter is plotted in Figure 6-2 as the function of the initial cavity length of the sensor probe, where the wavelength drift of the filter is assumed to be 0.07nm for the operating temperature range from -15°C to 55°C. As indicated in the figure, the error is proportional to the initial cavity length. For an initial cavity length of 25μm, the normalized error is about 0.8% of the full scale of measurement.

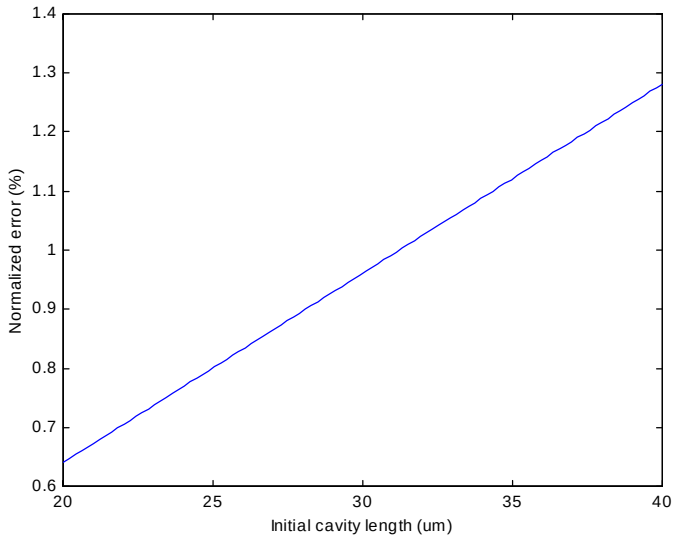

Figure 6-2. Normalized error induced by the wavelength drift of the filter

2. Residual interference fringe in the reference cannel

In order to reduce the error induced by the wavelength drift of the optical filter, and also to ensure a good fringe visibility of the signal channel, the initial sensor cavity length needs to be as small as possible. On the other hand, reducing the initial cavity length would generate an optical interference in the reference channel. This residual interference in the reference channel can cause an error to the measurement results as shown in the following discussion.

Assuming that the residual interference in the reference channel has a fringe visibility of γ_r, the output from the reference channel can be written as

$$I_1' = 2RI_0[1-\gamma_r \cos(\frac{4\pi}{\lambda}L)]. \qquad (6\text{-}21)$$

The output of the SCIIB system then becomes

$$s' = \frac{I_2}{I_1'} = \alpha \cdot \frac{1-\gamma_s \cos(\frac{4\pi}{\lambda} L)}{1-\gamma_r \cos(\frac{4\pi}{\lambda} L)}, \qquad (6\text{-}22)$$
$$\approx s[1+\frac{\gamma_r}{2}\cos(\frac{4\pi}{\lambda} L)]$$

where, s is the original SCIIB output as given by Equation (2-11).

3. Non-centered filtering

Both the SLED source and the optical bandpass filter used in the SCIIB system have a center wavelength of 1310nm. Assume that the actual center wavelength of the source is 3.1nm off from its nominal center wavelength. As schematically shown in Figure 6-3, this will have two effects on the output of the SCIIB system: 1) the center wavelength used to calculate the output of the reference channel in Equation (6-21) is no longer the same as the signal channel, and 2) the intensity of the signal channel will deviate from the original level of αI.

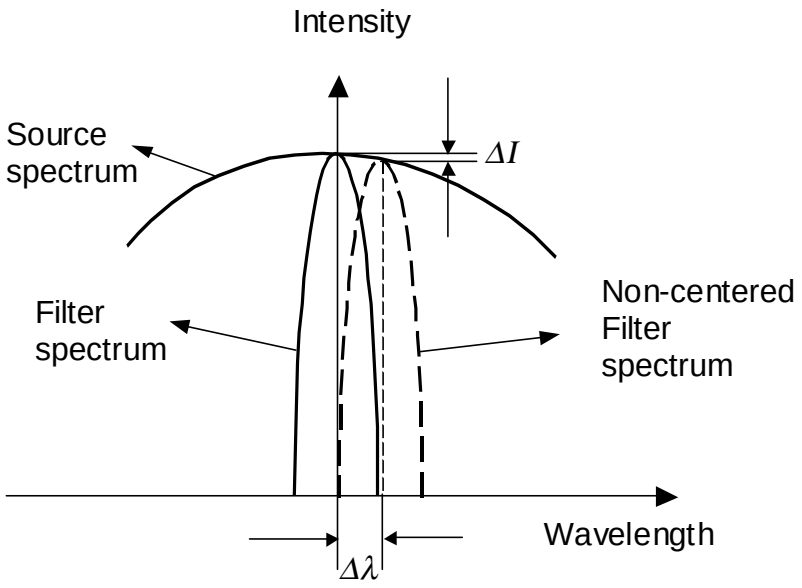

Figure 6-3. Schematic illustration of non-centered filtering

Therefore, Equation (6-22) can be modified to give the new output of the SCIIB system, given by

$$s' \approx s(1-\frac{\Delta I}{I_0})[1+\frac{\gamma_r}{2}\cos(\frac{4\pi}{\lambda-\Delta\lambda}L)], \tag{6-23}$$

where ΔI is the intensity change, and $\Delta\lambda$ is the center wavelength offset.

Both the residual interference in the reference channel and the non-centered filtering themselves will not cause measurement errors directly because once the system is calibrated these deviations are fixed. However, if the wavelength of the light drifts from the original spectrum, for example, because of the temperature induced drift of the source wavelength and the fiber bending induced spectral distortion, there will be errors resulting from these changes.

From Equation (6-23), the normalized measurement error resultant from the wavelength drift $\delta\lambda$ can thus be calculated by

$$\left.\frac{\delta s}{s}\right|_{\max} \approx \left\{ abs(\frac{1}{I_0}\frac{dI}{d\lambda}) + \frac{\gamma_r}{2}\cdot\frac{4\pi L}{\lambda^2} \right\}\Bigg|_{\lambda-\Delta\lambda} \cdot \delta\lambda, \tag{6-24}$$

where I is the normalized spectrum of the optical source, which can be modeled by the following Gaussian function

$$I(\lambda) = \frac{2I_0}{\sqrt{\pi}\Delta\lambda_0}\exp\left(-\frac{(\lambda-\lambda_c)^2}{\Delta\lambda_0{}^2}\right), \tag{6-25}$$

where I_0 is the total optical power, $\Delta\lambda_0$ is the e^{-1} half spectral width, and λ_0 is the central wavelength. Therefore, we have

$$\frac{1}{I_0}\frac{dI(\lambda)}{d\lambda} = -\frac{2(\lambda-\lambda_c)}{\sqrt{\pi}\Delta\lambda_0{}^3}\exp\left(-\frac{(\lambda-\lambda_c)^2}{\Delta\lambda_0{}^2}\right). \tag{6-26}$$

Figure 6-4 shows the calculated results of the normalized measurement error as a function of the wavelength drift given by Equation (6-24).

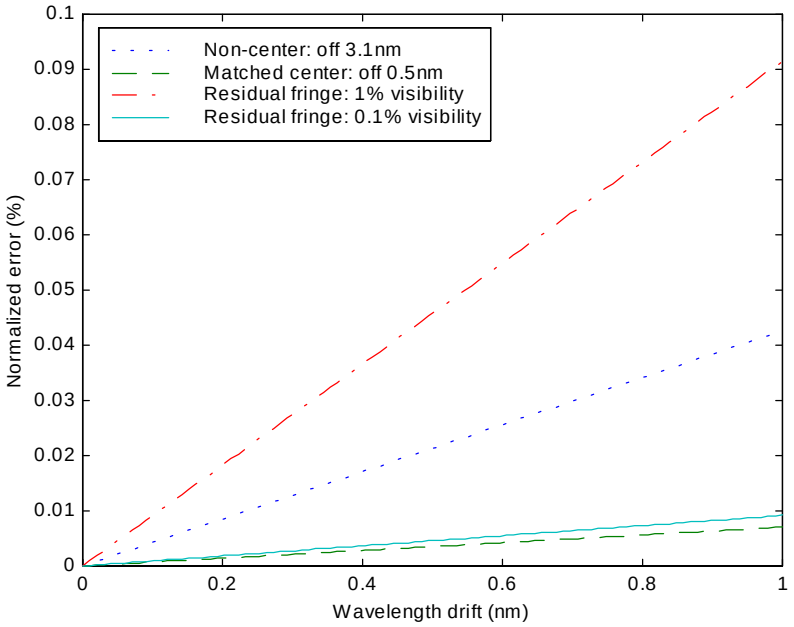

Figure 6-4. Normalized measurement error resultant from the residual interference in the reference channel and the non centered filtering, where the initial sensor cavity length is set to be $L_0=25\mu m$.

4. Source wavelength drift

The spectrum of a semiconductor optical source is temperature dependent. The change of temperature will cause changes to both the index of refraction of the active medium and the dimensions of the resonant cavity, and hence change the spectrum of the emitting light. To reduce the spectral fluctuation of the source, a thermo-resistor and a thermal electrical controller (TEC) are usually installed very close to the source chip. These two together with external controlling circuits form a feedback loop that helps to keep the chip temperature unchanged. With the help of the automatic thermo-electric cooling mechanism, the wavelength drift of the optical source can thus be minimized to the level of about 0.2nm.

5. Fiber Bending Introduced Spectrum Distortion

The spectrum of the light waves transmitted in a fiber will change when the fiber is bent. The fiber bending induced spectrum change (or the fiber bending loss spectrum) is a very complicated phenomenon. Although theoretical modeling of this process is possible, it will be easier and more direct to investigate this phenomenon experimentally.

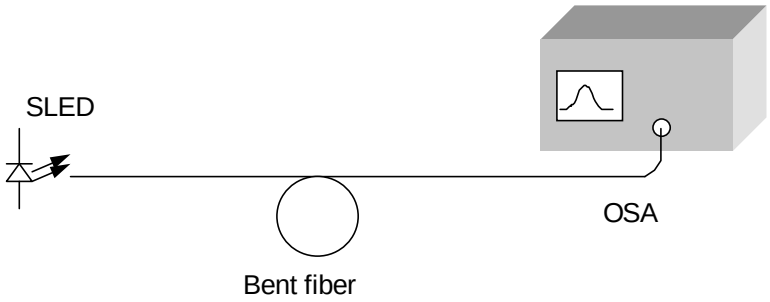

Figure 6-5. Experimental setup for the evaluation of fiber bending introduced spectrum change

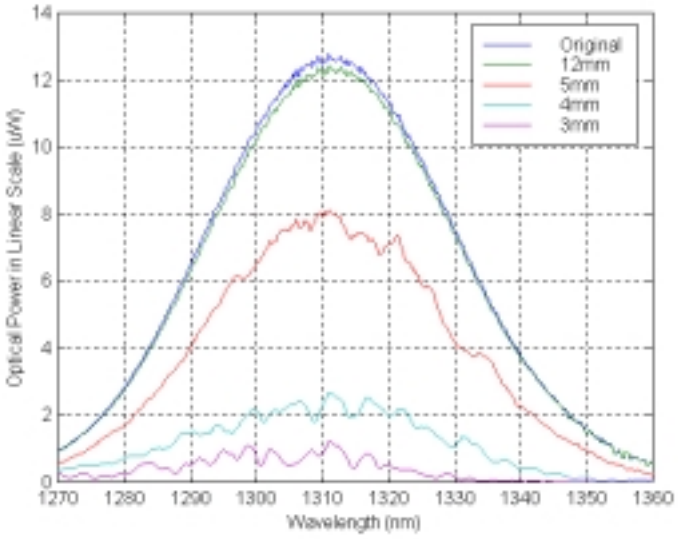

Figure 6-6. Bending induced spectrum change test results for regular telecom single-mode fiber

The schematic configuration of the experiment set-up is shown in Figure 6-5. The source used in the experiment was an Anritsu SLED. The output light from the source was transmitted through a section of single-mode fiber under test, and the transmitted spectrum was recorded by an optical spectrum analyzer (OSA). By manually bending the fiber to certain radii, we can study the bending introduced spectrum changes.

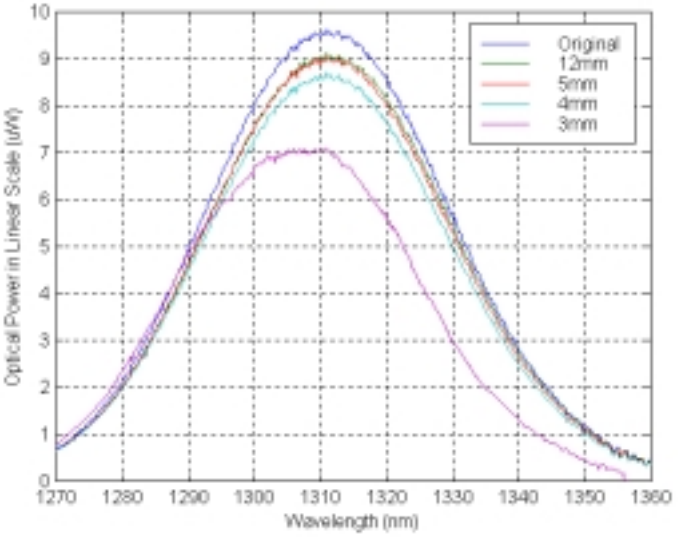

Figure 6-7. Bending induced spectrum change test results for bending insensitive single-mode fiber

Two types of single-mode fibers were evaluated experimentally. In the first experiment, a section of regular telecom single-mode fiber (SM28^{TM} fiber made by Corning Inc.) was used to run the test. The fiber was bent to a series of radii from 12mm to 3mm. The smallest bend that might be encountered when the sensor is deployed in an oil well is about 12mm. The typical spectra of light transmitted in the original and the bent fiber are plotted in Figure 6-6. Similar tests were also conducted using a section of bending insensitive single-mode fiber at 1300nm (purchased from Spectran Communication Fiber Technologies, Inc.), with the recorded spectra shown in Figure 6-7.

The optical interference of a broadband source is the contribution of each spectral component. For the purpose of evaluating the spectral distortion induced phase shift to the interference signal, the change of the effective central wavelength can be calculated from the recorded spectrum data. The calculated typical effective center wavelength change for regular single-mode fiber is about 0.3nm, and that of the bending insensitive fiber is about 0.2nm.

From the theories of fiber optics, the mode field radius $w(\lambda)$ of a step-index single-mode fiber can be approximated by [104]

$$w(\lambda) = a\left(0.65 + \frac{1.619}{V^{3/2}} + \frac{2.879}{V^{6}}\right), \tag{6-27}$$

where the electric filed of the guided mode is assumed to have a Gaussian distribution in shape, and V is the normalized frequency of the fiber, defined as

$$V = \frac{2\pi}{\lambda} a\sqrt{n_1^{\,2} - n_2^{\,2}}\,. \tag{6-28}$$

Here, a is the core radius, n_1 and n_2 are the refractive indices of the core and cladding respectively.

Examining Equation (6-27) and (6-28) reveals that the mode field diameter of a step-index single-mode fiber is proportional to the wavelength of the light. The light of longer wavelength will have a larger mode field diameter when it is transmitted in the fiber. Intuitively, the larger the mode field diameter, the higher loss it will be when the fiber is under bending because the optical energy is less confined inside the waveguide. This explains qualitatively why the long wavelength end of the spectra suffers larger loss compared to the short wavelength end, as shown in Figures 6-6 and 7-7. Because the mode field diameter of the regular telecommunication fiber is larger than that of the bending insensitive fiber, the loss of the regular fiber is higher than that of the bending insensitive fiber.

Bending a single-mode fiber can also cause the coupling between the guided mode and the cladding modes. The coupling between modes results in the transfer of energy between these modes, which is both wavelength and bending status dependent. Within the spectral range of the source, the coupling can be in favor of certain wavelength components than others depending on the status of bending. This explains the ripples in the transmitted spectrum when fiber is under bending.

In general, comparing the experimental results shown in Figures 6-6 and 6-7, the distortions of the spectrum in the bending insensitive fiber are smaller than that of the regular telecom fiber with the same bending radius. Even under severe bending, the transmitted spectrum of the bending insensitive fiber still does not exhibit spectral ripples. The larger distortion of the spectrum in regular telecom fibers is mainly due to the large mode field diameter of the waveguide. However, the difference between these two fibers is small for a relatively large bending radius (>12mm).

6.2.2 Change of SOP Induced Noise

The SLED used in the SCIIB system outputs almost linearly polarized light. As the light propagates inside the SMF, the state of polarization will change because of both intrinsic birefringence and extrinsic birefringence. Although the fiber Fabry-Perot sensor probe is polarization insensitive, the receiving optics of the SCIIB system is however polarization dependent. This is largely due to the residual polarization dependence of the optical beamsplitter.

1. Residual polarization sensitivity of the beamsplitter

The SCIIB receiving optics uses low polarizing cubic beamsplitter (made by OptoSigma Inc.) with a central operating wavelength of 1310nm to separate two channels for signal and reference. As shown in Figure 6-8, the beamsplitter has a residual polarization dependence of about 10% in the wavelength range (1250nm-1350nm). This will result in

the non-constant splitting ratio that is dependent on the state of polarization of the input light.

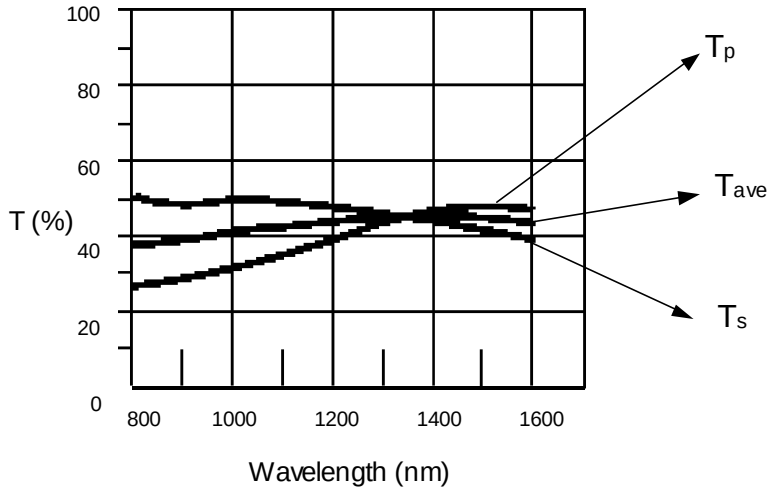

Figure 6-8. Transmission characteristics of the beamsplitter

Assuming that the splitting ratio of the beamsplitter as a function of the input SOP is given by

$$r(SOP) = \frac{I_1(SOP)}{I_2(SOP)} \neq 1:1, \tag{6-29}$$

the SCIIB output thus becomes

$$\begin{aligned} s' &= r(SOP)s \\ &= r(SOP)\alpha[1-\gamma\cos(\frac{4\pi}{\lambda}L)] \end{aligned}. \tag{6-30}$$

As indicated in Equation (6-30), the change of SOP will directly cause a normalized measurement error which can be calculated as

$$\frac{\Delta s}{s} = r(SOP) - 1. \tag{6-31}$$

From Figure 6-8, the maximum deviation of *r(SOP)* from its desired value (1:1) can reach 10% if the SOP of the light input to the beamsplitter changes from one polarization (*p*) to another (*s*). Therefore, the change of SOP can potentially introduce a normalized measurement error as large as 10%.

2. Polarization of single-mode fibers

If the fiber is perfectly circular with circularly symmetric refractive index distribution, the two LP_{01} (or HE_{11}) modes will be perfectly degenerate. That is both x-polarized (*Ey=0*) and y-polarized (*Ex=0*) LP_{01} modes have the same propagation constant [94,95]. However, actual fibers generally exhibit some ellipticity of the core and/or some anisotropy in the refractive index distribution due to anisotropic stresses. This results in two different propagation constants for the x-polarized (β_x) and y-polarized (β_y) LP_{01} modes, leading to perturbations of the state of polarization of the light transmitted by the fiber. The birefringence of the fiber ($\Delta\beta$) is usually defined as

$$\Delta\beta = \beta_y - \beta_x \ . \tag{6-32}$$

Based on the different mechanisms, the birefringence of the optical fiber can be divided into two major categories [96]. One is called the intrinsic birefringence which is caused by the ellipticity of the fiber shape or the anisotropy of the refractive index due to the built-in stress during the manufacturing process [97]. Another is the extrinsic birefringence which is caused by the external disturbance induced stress such as bending [98], lateral tension [99] and twist [100].

3. Stress induced birefringence of single-mode fibers

The stress applied to the fiber will cause additional birefringence through the photoelastic effect. The formula used calculate the stress induced normalized birefringence is given by [96]

$$B = \frac{\Delta\beta}{\bar{\beta}} = -n_1^{\,2}\,\frac{p_{11} - p_{12}}{2}\sigma \ , \tag{6-33}$$

where, n_1 is the refractive index of the fiber core, $p_{11} = 0.12$ and $P_{12}=0.27$ are the usual photoelastic coefficients of silica glass, σ is the stress applied to the fiber.

Because the materials used to manufacture optical fibers have different thermal expansion coefficients, it is possible to build anisotropic stresses into the fiber which lead to birefringence. The intrinsic thermal stress induced birefringence can be calculated through the following equation,

$$B = \frac{\Delta\beta}{\bar{\beta}} = -n_1^{\,2}\,\frac{p_{11} - p_{12}}{2}(s_2 - s_1)(T_a - T_g)\,, \tag{6-34}$$

where s_2 and s_1 are the thermal expansion coefficients of the cladding and the core, respectively, and T_a-T_g is the difference between the ambient temperature and the manufacturing temperature of the fiber (i.e. the temperature of glass softening).

For silica doped with a dopant *d*, we can write

$$s[(d)] = (d)s_d \; + \; [1\text{-}(d)]s_0 \;, \tag{6-35}$$

where (*d*) is the molar concentration of the dopant *d*, s_d is its thermal expansion coefficient, and s_0 is the thermal expansion coefficient of silica. Typical values are

$s_0 = 5 \times 10^{-7}$,

d = GeO_2, $s_d = 7 \times 10^{-6}$,

d = P_2O_5, $s_d = 14 \times 10^{-6}$,

d = B_2O_3, $s_d = 10 \times 10^{-6}$.

With above typical values, the thermal stress induced birefringence can be calculated for different single-mode fibers using Equation (6-34) and (6-35). Typical normalized birefringence for regular single-mode fibers is between 0.06% and 0.3%.

4. Fiber bending induced SOP change

Once the fiber has been manufactured, externally applied stresses can also lead to induced birefringence through the photoelastic effect. When a fiber of outside radius *a* is bent with a radius $R>>a$, the induced birefringence $\Delta\beta = \beta_y - \beta_x$ can be expressed as

$$B_b = \frac{\Delta\beta_b}{\beta} = 0.25 n_1^2 (p_{11} - p_{12})(1+\upsilon)(\frac{a}{R})^2, \tag{6-36}$$

where υ is the Poisson's ratio of silica glass (υ*=0.17*). With the values p_{11}*=0.12* and p_{12}*=0.27* for silica glass, we obtain

$$B_b = -0.093(\frac{a}{R})^2. \tag{6-37}$$

This birefringence is due to a second-order stress compared to the dominant longitudinal stress, which has no effect because of symmetry. Again the maximum normalized birefringence that can be induced this way is limited by the tensile strength of the fiber. The strain on the external outer surface of the fiber is given by *a/R* and should not exceed about 2% for laboratory experiments. The corresponding limit for $|B_b|$ is about 1.5×10^{-6}.

The single-mode fiber in the status of bending can be viewed as a wave plate with its phase delay unknown due to the random number of bends and the random value of bending radius when the fiber is deployed into an oil well. For a linearly polarized input light, the SOP of the output light can thus be arbitrary (linearly polarized in any possible direction, circularly polarized, or elliptically polarized). To be conservative, the maximum estimated error of 10% as given by Equation (6-31) is valid for the entire case.

6.3 System performance optimization

In the two previous sections, the electronic and the optical noises of the SCIIB sensor system were studied in detail. The typical values of these errors are summarized in Table 6-3 for comparison. It is shown in the table that the electronic noise is very small compared to the optical noises. Therefore, the emphasis of the system optimization should be placed on the improvement of the optical system. Among the 4 items of optical noises, the change of SOP has the most significant effect on the system performance. This noise therefore must be reduced. The noises resultant from the residual interference in the reference channel and the non centered filtering can also be reduced by the proper

design of the system. However, the temperature dependence of the optical bandpass filter is an almost fixed error which little can be done due to the limited commercial availability of the components.

Table 6-3. Typical electronic and optical noises for the SCIIB sensor system

Noise sources	Typical Values
Electronics noises	0.00115%
Optical noises	
1. Spectral drift of the optical bandpass filter	0.8% (from -15°C to 55°C @ L_0 = 25μm)
2. Residual interference in the reference channel	0.0458% (0.5nm wavelength drift @ L_0 = 25μm)
3. Non centered filtering	0.0213% (0.5nm wavelength drift)
4. Change of SOP	10%

6.3.1 Optical system optimization

1. Discussions on the residual interference in the reference channel

As indicated in Equation (6-24) and shown in Figure 6-4, the measurement error resultant from the residual interference in the reference channel is proportional to the fringe visibility of the residual interference (γ_r), which is inversely proportional to the initial sensor cavity length. Therefore, increasing the initial sensor cavity length will help to reduce the residual fringe visibility in the reference channel and hence reduce the corresponding measurement error.

On the other hand, Equation (6-24) also reveals that the measurement error is also proportional to the initial cavity length (L_0). The longer the initial sensor cavity, the larger the measurement error. Therefore, the smallest measurement error will result from the balance between these two effects. In order to find an optimal initial sensor cavity length, several sensors with different cavity lengths were made. The experimental results and the theoretical simulation as shown in Figure 2-4 through 2-7 indicate that the visibility of

the residual interference in the reference channel decreases very fast as the cavity length increases before it reaches 20μm. However, after 25μm, the visibility decreases very slowly as the sensor cavity length increases. Therefore, the sensor cavity length is chosen to be 25μm in the final design.

2. Reduction of the non-centered filtering induced error

As shown in Figure 6-4, measurement error is proportional to the offset between the center of the optical bandpass filter and that of the source spectrum. The closer the match of the two center wavelengths, the smaller the measurement error will be. To reduce the mismatch between these two center wavelengths, the optical bandpass filter was rotated by an angle of about 10° from the normal incidence. By doing this, the mismatch between the two center wavelengths was reduced within 0.5nm. The corresponding measurement error was reduced from 0.0213% to 0.0035% by estimation.

3. Reduction of the change of SOP induced error

The change of SOP can cause a large measurement error mainly through the residual polarization sensitivity of the beamsplitter used in the SCIIB system. Due to the limitation of the technology in making the beamsplitter, it is difficult to find a beamsplitter with a splitting ratio purely independent of the state of polarization of the input light. However, if the input light is totally unpolarized natural light, even using a polarization-sensitive beamsplitter, the splitting ratio can be maintained constant and the polarization issue will not be a concern at all. This naturally leads us to use a depolarizer to minimize the change of SOP induced error.

By definition, a depolarizer is an optical device transforming polarized (or partially polarized) light into naturally unpolarized or depolarized light. Before the detailed discussion of a depolarizer, let’s review the mathematical tools used to describe the polarization properties of light.

The state of polarization of light can be described using Stokes parameters and Muller matrices when only the optical intensity (other than the optical field) is of interest [101-103]. The Stokes parameters are defined as:

$$\begin{cases} S_0 = A_x^{\,2} + A_y^{\,2} \\ S_1 = A_x^{\,2} - A_y^{\,2} \\ S_2 = 2A_xA_y\cos\phi \\ S_3 = 2A_xA_y\sin\phi \end{cases}, \tag{6-38}$$

where A_x and A_y are the optical field intensities along x and y-axes respectively, and ϕ is the phase difference between these two components.

The sStokes parameters have their physical meanings. S_0 is the total intensity of the light. S_1 describes the amount of linear horizontal or vertical polarization. S_2 describes the amount of linear +45° or -45° polarizations. S_3 describes the amount of right or left circular polarization contained within the beam. For mathematical convenience, the Stokes parameters are usually arranged in a column matrix which is called the Stokes vector.

The Stokes vector not only is useful for describing the polarization state of the light, it also can be used for describing the degree of polarization (P), which is defined to be

$$P = \frac{I_{pol}}{I_{tot}} = \frac{\sqrt{S_1^{\,2} + S_2^{\,2} + S_3^{\,2}}}{S_0}, \qquad 0 \le P \le 1 \tag{6-40}$$

where, $I_{pol} = \sqrt{S_1^{\,2} + S_2^{\,2} + S_3^{\,2}}$ is the optical intensity of the polarized part of the light. Thus, $P = 0$ indicates that the light is unpolarized, $P = 1$ that the light is completely polarized, and $0 < P < 1$ that the light is partially polarized.

Another mathematical tool associated with the Stokes vector is the Muller matrix (M), which is a 4×4 matrix and has been used to describe the specific function of an optical

component in terms of its properties of alternating the state of polarization of the input light. The process of the light propagating through an optical component in terms of its state or degree of polarization changes can thus be described by two Stokes vectors and the Muller matrix, which is given by

$$S_o = M \cdot S_i, \tag{6-41}$$

where, S_o is the Stokes vector of the output light, M is the Muller matrix describing the optical component, and S_i is the Stokes vector of the input light.

Using the definitions above, we can now model an optical depolarizer in terms of Stokes vectors and Muller matrices. Mathematically, a depolarizer with a Muller matrix M will transfer the polarized (or partially polarized) light with its Stokes vector given by S to the unpolarized output S' so that the following equation holds,

$$S' = \begin{pmatrix} S_0 \\ 0 \\ 0 \\ 0 \end{pmatrix} = M \begin{pmatrix} S_0 \\ S_1 \\ S_2 \\ S_3 \end{pmatrix}, \tag{6-42}$$

where, S_0 is the optical intensity, S_1, S_2 and S_3 could be any arbitrary numbers.
Therefore, the Muller matrix that can fulfill Equation (6-42) must be

$$M = \begin{pmatrix} 1 & 0 & 0 & 0 \\ 0 & 0 & 0 & 0 \\ 0 & 0 & 0 & 0 \\ 0 & 0 & 0 & 0 \end{pmatrix}. \tag{6-43}$$

However, it is very difficult to find an optical component that can fulfill the Muller matrix expressed by Equation (6-43). Only the phenomenon of diffusion by powders, ground optical surfaces or opal glasses is possible to fully depolarize the light. Then the difficulty comes to how to collect the light diffracted in emerging directions covering a wide angular domain.

The solution to above difficulty is the pseudo-depolarizers or polarization states mixer. For example, Lyot depolarizer, which has an effective function similar to Equation (6-43) when used to transfer a broadband light source and detected by a wide-spectrum detector. In this case, the Mueller matrix appears as a function of the wavenumber $k = 2\pi/\lambda$, i.e. $M(k)$. Mathematically, the process can be modeled by

$$\int_k (M(k) \cdot S) dk = \begin{pmatrix} S_0 \\ S_1' \\ S_1' \\ S_1' \end{pmatrix}. \tag{6-44}$$

Let's consider a plane wave having a Gaussian spectrum centered at k_0 and a spectral width Δk, which can be expressed as

$$I(k) = I_0 \exp\left(-\frac{(k-k_0)^2}{\Delta k} \right). \tag{6-45}$$

Assume that the input light has a Stokes vector S, which is a function of the wavenumber given by

$$S(k) = \begin{pmatrix} 1 \\ S_1 \\ S_2 \\ S_3 \end{pmatrix} I(k), \tag{6-46}$$

where S_1, S_2, and S_3 are arbitrary.

The Lyot depolarizer is made of two optical crystals (L_1 and L_2) cut from the same material. The neutral lines of crystal L_2 are aligned perfectly with the bisectors of the neutral lines of L_1. These two optical crystals can be characterized by the optical phase delays δ_1 and δ_2. The Muller matrix of the Lyot depolarizer can thus be expressed by [103]:

$$M(k,\delta_1,\delta_2)=\begin{pmatrix}1 & 0 & 0 & 0\\ 0 & \cos(2\pi k\delta_2) & \sin(2\pi k\delta_1)\sin(2\pi k\delta_2) & -\cos(2\pi k\delta_1)\sin(2\pi k\delta_2)\\ 0 & 0 & \cos(2\pi k\delta_1) & \sin(2\pi k\delta_2)\\ 0 & \sin(2\pi k\delta_2) & -\sin(2\pi k\delta_1)\cos(2\pi k\delta_2) & \cos(2\pi k\delta_1)\cos(2\pi k\delta_2)\end{pmatrix}. \quad (6\text{-}47)$$

The Stokes parameters S_1', S_2', and S_3' of the emerging light can thus be calculated by using Equation (6-44). It can be shown that the Stokes parameters S_1', S_2', and S_3' in Equation (6-44) will become zero if the following conditions are satisfied,

$$\begin{cases}\delta_1 >> \dfrac{1}{\Delta k}\\ \delta_2 \geq 2\delta_1\end{cases}. \quad (6\text{-}48)$$

Equation (6-48) indicates that 1) the phase lag of the first crystal must be larger than the coherence length L_c of the light, and 2) the second crystal (L_2) must be more than twice as thick as the first one (L_1). If these two conditions are satisfied, the light emerging from the Lyot depolarizer will be effectively unpolarized when it is seen by a wide-spectrum detector.

All the above discussions suggest that if a Lyot depolarizer can be installed right before the light propagating into the beamsplitter so that the beamsplitter and the photodetectors behind effectively see unpolarized light emerging from the depolarizer no matter how the state of polarization changes in front of the depolarizer. Thereafter the splitting ratio of the beamsplitter eventually becomes insensitive to the polarization disturbance associated with the fiber bending or other causes.

In our system, an optical fiber-based Lyot depolarizer was used, which has two polarization maintaining fibers replacing the two optical crystals described above. The optical fiber Lyot depolarizer, made by the Noah Industries, Inc., has an extinction ratio of 20dB (100:1). It is estimated that the change of SOP induced measurement error can thus be reduced from 10% to 0.1%.

6.4 Other System Optimization Measures

In addition to the electronic and optical noises discussed in Sections 6.2 and 6.3, there are other sources of errors that would potentially affect the performance of the system. These include the dark current induced bias and the non-linearity caused by the unmatched electronic amplifiers. The methods to minimize the errors resultant from these two are presented in this section.

6.4.1 Correction for the dark current induced bias

The dark current of the photodetector will add a constant bias to photocurrent of interest. Although the dark current of the InGaAs detector used in the SCIIB system is very small (in the order of 15 pA), the resultant bias can affect the measurement result to some extends due to the relatively low optical power reflected from the sensor probe. To investigate the dark current induced error, let's assume that the signal currents of the two channels are I_{p1} and I_{p2} with the corresponding the dark currents of I_{d1} and I_{d2} respectively. The SCIIB ratio can thus be written as

$$s' = \frac{I_{p1} + I_{d1}}{I_{p2} + I_{d1}} = \frac{I_{p1}}{I_{p2}} + \frac{I_{d1}}{I_{p2}} + O^2, \tag{6-49}$$

where O^2 is the second or higher order terms of I_{d1} and I_{d2}, which will be neglected from the analysis. The corresponding deviation from the ideal output ratio is

$$\Delta s = s' - s \approx \frac{I_{d1}}{I_{p2}}. \tag{6-50}$$

Therefore, the normalized error resultant from the dark current bias within the linear range of operation becomes:

$$\frac{\Delta s}{s} = \frac{I_{d1} / I_{p2}}{I_{p1} / I_{p2}} = \frac{I_{d1}}{I_{p1}}, \tag{6-51}$$

where, I_{p1} should be confined in the linear operating range of the system.

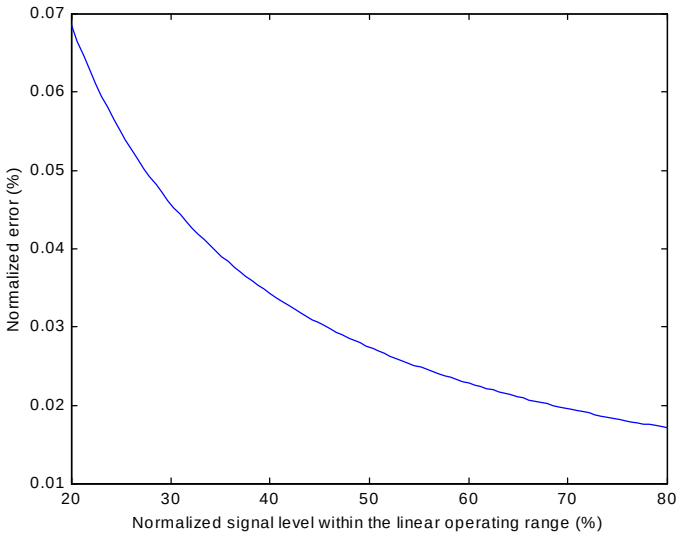

Figure 6-9. Normalized measurement error resultant from the dark current bias

The normalized error is plotted as a function of the normalized signal level in Figure 6-9, where the average signal current is assumed to be 54.7nA and the dark current is 15pA adopted from Table 6-1. As shown in the figure, the measurement error resultant from the dark current bias can reach 0.07% when the signal level is low (close to the valley of the interference fringe).

Because the final ratio function is performed digitally by the host computer, the correction of the dark current bias becomes relatively easy. We can record in advance the output voltage of the two SCIIB channels when the optical source is turned off. The dark current is almost a constant when the photodetector is chosen. Therefore, the dark current bias can be eliminated from the final ratio using the following equation

$$s = \frac{V_1 - V_{d1}}{V_2 - V_{d2}}, \tag{6-52}$$

where V_1 and V_2 are the output signal voltages, and V_{d1} and V_{d2} are the recorded dark-current voltages of the two channels respectively.

6.4.2 Balance the optical power of the two channels

Because of the very large amplification factors of the transimpedance amplifiers used in the SCIIB system, the nonlinearity of the amplifiers could be a concern. However, the nonlinearity of the amplifiers can be compensated if the two amplifiers are exactly the same. Another reason to match these two amplifiers is the consideration of the temperature dependence. The resistances of the feedback resistors used in the transimpedance amplifiers will change as the environmental temperature fluctuates. If they changes in the same direction and in the same amount, by taking the ratio of the two outputs, the temperature fluctuation will have very little effects on the system output.

To be able to match the two transimpedance amplifiers, we need to balance the optical power input to the two photodetectors. Because an optical bandpass filter is used in the signal channel to increase the coherence length, the signal channel will see less optical power than the reference channel. In order to balance the two channels in terms of the optical power, an optical neutral density filter can be inserted into the reference channel with a flat spectral response within the spectral range of interest, which introduces additional attenuation to the optical intensity of the reference channel.